Physica E: Low-dimensional Systems and Nanostructures 105 (2019) 125–138

Contents lists available at ScienceDirect

Physica E: Low-dimensional Systems and Nanostructures

journal homepage: www.elsevier.com/locate/physe

Exact ray theory for the calculation of the optical generation rate in optically thin solar cells

M.A. Brandsrud[a,1], E. Seim[a,*,1], R. Lukacs[a], A. Kohler[a], E.S. Marstein[c,d], E. Olsen[a], R. Blümel[b]

[a] Norwegian University of Life Sciences, Faculty of Science and Technology, Drøbakveien 31, 1432 Ås, Norway
[b] Wesleyan University, Department of Physics, 265 Church Street, Middletown, 06459, CT, USA
[c] Institute for Energy, Department of Solar Energy, Instituttveien 18, 2007, Kjeller, Norway
[d] University of Oslo, Department of Physics, Gunnar Randers vei 19, 2007, Kjeller, Norway

A B S T R A C T

There is a profound duality between rays and waves. In fact, 70 years ago, in the context of quantum mechanics, Feynman showed that rays, properly equipped with phases and correctly summed, provide exact solutions of the quantum mechanical wave equation. In this paper, constructing explicit, exact ray solutions of the one-dimensional Helmholtz equation as a model for optically thin solar cells, we show that the ray-wave duality is also exact in the context of the electromagnetic wave equations. We introduce a complex index of refraction in order to include absorption. This have so far not been treated in the quantum ray-splitting literature. We show that inclusion of exact phases is mandatory and that a ray theory without phases may result in amplitude errors of up to 60%. We also show that in the case of multi-layered solar cells the correct summation order of rays is important. Providing support for the notion that rays provide the "skeleton" of electromagnetic waves, we perform a Fourier transform of the (experimentally measurable) solar cell reflection amplitude, which reveals the rays as peaks in the optical path length spectrum. An application of our exact ray theory to a silicon solar cell is also provided. Treating the one-dimensional case exactly, our paper lays the foundation for constructing exact ray theories for application to solar cell absorption cross section in two and three dimensions.

1. Introduction

In the quest for cheaper and cheaper solar cells, the solar cell community is continuously on the lookout for ways to decrease material costs. It is well known that in order to produce thinner solar cells with the same absorption properties as their thicker counterparts, absorption of optically thin solar cells may be enhanced by the use of nano-layering or by nano-structuring [1,2]. In order to investigate the nature of the absorption enhancement of optically thin solar cells by nano-layering or structuring, full wave calculations have been employed [3,4]. Shape resonances such as whispering gallery modes in spherical nanostructures have been considered as one possible cause for the absorption enhancement [5]. As another possible cause for the absorption enhancement, the coupling of modes in periodic nano-structures has been considered [6]. While absorption enhancement by nano-layering and nano-structuring has been demonstrated both experimentally [7] and numerically [8], the origins of the absorption enhancement mechanisms are not completely understood. Handy tools for investigating wave propagation and absorption properties of electromagnetic radiation in complex nano-structures are required for achieving a deeper understanding.

In the short wavelength limit, i.e., when the wavelength is small compared to the size of the structures used for absorption enhancement (e.g in micro-structured materials), ray tracing has been employed as an approach for investigating wave propagation and absorption enhancement in solar cells since the 1980s [9–11], when the optical performance of various solar cell designs was evaluated using ray-tracing techniques for the computation of the reflectance, transmittance and absorption. Since then, several numerical codes [12–19] and methods were developed, such as the Monte Carlo ray tracing method [20], the polarization ray tracing technique [21,22], the ray tracing combined with transfer matrix theory [23] and ray tracing combined with image processing [17]. Starting with one-dimensional modelling [24], these methods were later extended to two and three dimensions [25–28].

Ray tracing methods have been shown to explain the trapping of rays in solar cells. However, ray tracing fails to explain resonance effects in nano-structured materials such as whispering gallery modes. The reason for this deficiency is obvious: In order to describe resonance effects in layered thin films or films with nano-structures, the wave nature of the electromagnetic radiation needs to be taken into account, while the classical ray picture in electrodynamics is used to study the propagation of electromagnetic waves in terms of rays for cases where the wavelength of the electromagnetic radiation is short compared to changes of the media in which the electromagnetic radiation is

* Corresponding author.
E-mail address: e.seim.es@gmail.com (E. Seim).
[1] Contributions to the publication are considered equal.

https://doi.org/10.1016/j.physe.2018.08.018
Received 4 July 2018; Received in revised form 22 August 2018; Accepted 31 August 2018
Available online 05 September 2018

propagating. This is not the case for optically thin solar cells with nano-layers and nano-structures, where the optical properties of the material change on a scale which is comparable to the wavelength of light.

In the field of quantum theory, a ray theory that takes into account the wave nature is readily available. In quantum mechanics, the ray-wave duality leads to the important field of semiclassical methods [29,30], which attempts to solve the quantum Schrödinger equation on the basis of classical particle trajectories. Using rays to solve the wave equations is tempting since it is usually much more straightforward to solve the ordinary differential equations determining the dynamics and geometry of rays, than solving the wave equations, which requires the solution of partial differential equations of continuous media. In order to obtain an exact result on the basis of rays, the rays need to be associated with phases; if for each ray the correct phases can be determined, the wave-ray duality is exact and the wave equations may be solved on the basis of rays. Since in this case, the ray theory solves the Helmholtz equation exactly, the ray theory can also correctly handle resonances caused by the wave nature of light. In addition, we introduced a complex refractive index in the ray theory allowing to treat absorption, which so far has not been introduced in quantum ray-splitting literature.

Only recently, in the field of solar cells, attempts that include phases have been reported [31].

In order to increase the understanding of the behavior of light in nano-layered and nano-structured solar cells, we present a ray theory that yields an exact description of the behavior of light in one-dimensional systems and allows to explain absorption enhancement due to nano-layering and nano-structuring.

In order to demonstrate the new theory, we study the optical generation rate of optically thin solar cells, modeled as vertical stacks of thin (absorbing) dielectric films, under normal incidence of light. In sections 2 and 3 we show that in this case, with or without a mirror behind the stack, Maxwell's vector equations are equivalent with a one-dimensional scalar Helmholtz equation, which we solve with our exact ray theory. We will use the scalar theory throughout this paper. In order to model absorption, we use a complex index of refraction. In section 4 we introduce a hierarchical scheme of summing rays as a convenient method of keeping track of rays bouncing off of and transmitting through different dielectric layers of the solar cell. We also show that including only the simplest rays already yields an excellent approximation of the exact solution of the wave equation. In Section 5 and 6 we show that both summation order and phases are important in our ray theory. We show in section 7 that the signature of the most important rays appears as peaks in the Fourier transform of the reflection amplitude of a flat solar cell. In section 8 we demonstrate how our ray theory can be used for materials with practical importance within the solar cell field. In Section 9 we discuss our results; we summarize and conclude our paper in Section 10.

Our method can be extended for use in two and three dimensions. The theory describes the optical properties of a device and is based on the imperative that phases need to be included to arrive at a useful ray theory.

2. The scalar wave model for a one-dimensional film

In order to develop a ray theory for studying absorption enhancement in optically thin solar cells, we consider one-dimensional systems in which electromagnetic radiation is propagating towards a region consisting of one or more parallel layers of different materials. In this section we will introduce one-dimensional model system that we will use for illustration throughout the paper. In all cases, we consider the propagation direction as normal to the surfaces of the materials. Since we want to develop model systems for optically thin solar cells, we study cases where one or more of the layers consist of energy-converting materials. We describe the incoming electromagnetic wave by a plane wave. Since we consider only normal incidence, the system can be fully described by a scalar wave function, ψ [32].

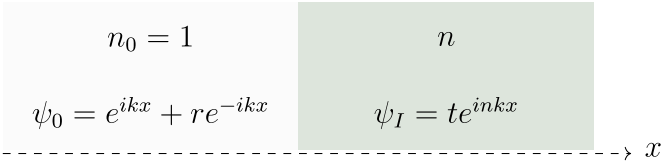

Fig. 1. Schematic description of a half-space problem, where the left half space is vacuum ($n_0 = 1$) and the right half space is material. A plane wave is propagating towards a boundary between vacuum ($n_0 = 1$) and an arbitrary dielectric material with refractive index $n = n_r + in_i$. The imaginary part n_i of the refractive index is set to zero if the dielectric material is non-absorptive. The waves are propagating in x-direction, normal to the surface. ψ_0 and ψ_I are the scalar wave functions in the two regions, $k = 2\pi/\lambda$ is the angular wave number in vacuum, and λ is the vacuum wavelength. r and t are here the reflection and transmission amplitudes for the plane wave in this system; the amplitude of the incoming plane wave is set to one.

The first and simplest system we will investigate is a system consisting of a single film. By evaluating the scalar wave function for one single film, where the material of the film is an energy-converting material with complex refractive index $n = n_r + in_i$, we can understand the occurrence of interference maxima and investigate how these are related to the enhancement of the absorption cross section. The interference maxima are resonances akin to the whispering gallery resonances that occur in spherical particles used for nano-structuring solar cells, which lead to an enhancement of the electric field and the absorption properties of the solar cells.

The reflection probability R at the boundary between two materials is calculated as $R_b = |r|^2$, where r is the amplitude of the reflected wave (see Fig. 1). By requiring a continuous scalar wave function and a continuous first derivative of the scalar wave function at the boundary, we can derive an expression for R_b for the case illustrated in Fig. 2 [33], i.e.,

$$R_b = \frac{(1 - n_r)^2 + n_i^2}{(1 + n_r)^2 + n_i^2}. \tag{2.1}$$

The probability for transmission at the boundary for the system in Fig. 1, T_b, is given by $T_b = |t|^2 = 1 - R_b$.

We start by evaluating two simple systems, namely a single film and a single film with a mirror, as shown in Fig. 2a and b, respectively.

We require that the wave function and its first derivative are continuous at the boundaries and that the wave function is zero at the surface of the mirror. We derive the transmission probability $T = |t|^2$ and the reflection probability $R = |r|^2$ for the systems, where t and r are the amplitudes of the transmitted and reflected plane waves, respectively. For the single-film case, shown in Fig. 2a, the reflection and transmission amplitudes are given by

$$r = \frac{i \sin(nka)[(nk)^2 - k^2]}{2nk^2 \cos(nka) - i \sin(nka)[(nk)^2 + k^2)]}, \tag{2.2a}$$

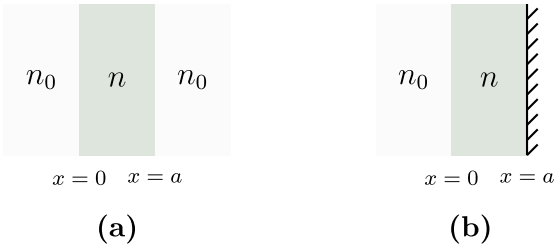

Fig. 2. Two simple single film systems. (a) A single film in vacuum and (b) a single film in vacuum with a mirror. The refractive index of the film is given by $n = n_r + in_i$. $n_0 = 1$ is the refractive index of vacuum, a is the thickness of the film.

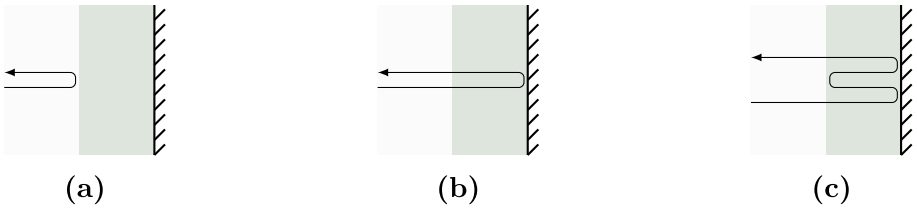

Fig. 3. Three types of rays encountered in a film-plus-mirror system. (a) The ray directly reflects from the surface. This ray does not contribute to the absorption cross section. (b) The simplest ray that contributes to the absorption cross section. The ray enters into the film is reflected from the mirror and exits. (c) A more complex ray contributing to the absorption cross section. This ray has two reflections from the mirror and one internal reflection from the film-vacuum boundary.

$$t = \frac{2nk^2 e^{-2ika}}{2nk^2\cos(nka) - i\sin(nka)[(nk)^2 + k^2]}, \tag{2.2b}$$

where $k = 2\pi/\lambda$ is the angular wave number in vacuum, λ is the vacuum wavelength, nk is the angular wave number in the film, n is the complex refractive index of the film, and a is the thickness of the film. If the film is non-absorptive, i.e., n is real, it is straightforward to show that Eqs. 2.2a and 2.2b lead to $R + T = |r|^2 + |t|^2 = 1$, i.e., all electromagnetic radiation entering the film is eventually leaving the film again.

In the case a mirror is present (see Fig. 2b), there is no transmission. Therefore the system can be characterized by the reflection amplitude alone, which in this case is given by

$$r = \frac{n\cos(nka) + i\sin(nka)}{n\cos(nka) - i\sin(nka)}. \tag{2.3}$$

If the film is non-absorptive, i.e., n is real, it follows immediately from Eq. (2.3) that $R = |r|^2 = 1$, i.e. again all electromagnetic radiation entering the film is eventually leaving the film.

We define the *absorption cross section* as the fraction of light that is absorbed and denote it by σ. In the two cases shown in Fig. 2, the film with and without the mirror, the expressions for σ are respectively given by

$$\sigma(\lambda) = 1 - R(\lambda), \tag{2.4a}$$

$$\sigma(\lambda) = 1 - (R(\lambda) + T(\lambda)). \tag{2.4b}$$

According to the definition of σ as the fraction of absorbed light, i.e., light that does not exit the solar cell, in addition to absorbed light that leads to beneficial photo current, σ contains all parasitic absorption processes, for instance the two-photon process [34,35].

The same procedure can be applied for film-systems without mirror. For a non-absorptive film, σ is zero. For the rest of this paper, we will focus exclusively on cases where a mirror is placed behind the film/films in order to model a solar cell system.

In an equivalent solar cell system the absorption cross section is the total amount of absorbed energy absorbed at a given wavelength λ. This is the maximal amount of energy that can potentially create electron-hole pairs at a given wavelength λ. Under normal operating conditions, if the total amount of absorbed energy is increasing, the number of the photo-electrons will also increase and this will lead to enhanced efficiency. When the absorption cross section is weighted by the AM1.5 solar spectrum, we obtain the *optical generation rate*, G_{opt}. The optical generation rate G_{opt} has been introduced to the solar cell field by Ferry et al. [36]. Since then it is used as the measure of the optical performance of various solar cell designs. In our case G_{opt} is given by

$$G_{opt}(\lambda) = \Gamma_{solar}(\lambda)\sigma(\lambda)A, \tag{2.5}$$

where $\Gamma_{solar}(\lambda)$ is the spectral weighting term and A is the surface area of the solar cell. In this paper we will evaluate $\sigma(\lambda)$ for our systems in order to get a fundamental understanding of how the optical resonances in the energy converting film increase the total amount of absorbed energy.

For a single film, or a stack of films, with different refractive indices, it is possible to analytically derive a formula for the absorption cross section from the probability current. This depends only on the absolute square of the scalar wave function inside of the film(s). To be specific, we consider the case of an array of films, described by a space-dependent complex refractive index $n(x) = n_r(x) + in_i(x)$. The complex refractive index $n(x)$ when the optical or the absorption properties of a material change. When a stack of films is illuminated from the front and backed by a mirror, the absorption cross section is given by

$$\sigma = 2k\int_0^w n_i(x)n_r(x)|\psi(x)|^2\,dx, \tag{2.6}$$

where the stack of films is assumed to be located in the interval $0 \le x \le w$ and the mirror is located at $x = w$. The details of the derivation are presented in Appendix B. Since for a single film with mirror both r and $\psi(x)$ are known explicitly (see Eq. (2.3) and Appendix B), it is straightforward in this case to show by explicit calculations that Eq. (2.6) holds (see Appendix C).

3. Exact ray theory for single films

In this section, we will show that it is possible to estimate the absorption cross section by considering and summing rays. Three examples of simple rays are shown in Fig. 3.

In order to calculate the total reflection amplitude r we need to sum up all possible rays in the film [37,38]. Every ray contributes to the total reflection amplitude and thereby to the absorption cross section with an amplitude and a phase. The reflection and transmission amplitudes of the ray depending on the side of the boundary the ray is hitting. Denoting by r_l and t_l the reflection and transmission amplitudes, respectively, for a ray originating from outside in the vacuum and transmitting into the film, and by r_r and t_r the reflection and transmission amplitudes, respectively, for a ray originating from inside of the film and traveling towards the vacuum, we obtain (see Appendix A):

$$r_l = \frac{1-n}{1+n}, \tag{3.1}$$

$$t_l = \frac{2}{1+n}, \tag{3.2}$$

$$r_r = -\left(\frac{1-n}{1+n}\right), \tag{3.3}$$

$$t_r = \frac{2n}{1+n}. \tag{3.4}$$

It is important to note that the amplitudes, eq. (3.1)–(3.4), remains exact if the refractive index, n, is complex. We hereby established a ray model that is able to describe absorption of electromagnetic radiation. In addition to the amplitudes, we need to include the phase that the ray collects when it transverses the film, i.e., each time it travels from the vacuum-film interface to the mirror or from the mirror to the interface. This phase collected when traveling through the distance a is given by e^{inka}. Further we have to include the phase $e^{i\pi}$ [39] caused by the mirror each time a ray is reflected by the mirror.

To introduce our procedure, we state the contribution to r from the three selected rays illustrated in Fig. 3. The result is

$$r = r_l + t_l e^{inka}e^{i\pi}e^{inka}t_r + t_l e^{inka}e^{i\pi}e^{inka}r_r e^{inka}e^{i\pi}e^{inka}t_r, \tag{3.5}$$

where the first term is the contribution of the ray illustrated in Fig. 3a,

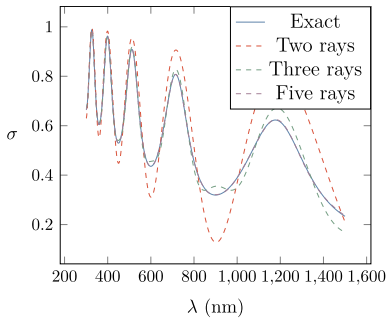

Fig. 4. Absorption cross section σ as a function of the wavelength λ for the system given in Fig. 2a. The blue line is calculated analytically with Eq. (2.3) and the ray model with Eq. (3.6) is used when the two (red dashed), three (green dashed line) and five (purple dashed line) simplest rays are included. The refractive index of the film in this system is 1.8 + 0.05i and the thickness is 500 nm. The wavelength ranges from 300 nm to 1500 nm. (For interpretation of the references to color in this figure legend, the reader is referred to the Web version of this article.)

the second term is the contribution from the ray illustrated in Fig. 3b, and the third term is the contribution from the ray illustrated in Fig. 3c. If we include all contributing rays, their total, exact contribution to r is given by

$$r = \eta + t_l t_r e^{i\pi} e^{2ink a} \sum_{\nu=0}^{\infty} (e^{i\pi} r_r e^{2ink a})^{\nu}. \tag{3.6}$$

By inserting the expressions for r_l, t_l, r_r and t_r, and with the help of the elementary summation formula for the geometric series, it turns out that r in Eq. (3.6) is equal to r in Eq. (2.3).

Whenever an energy-converting film is present, i.e., whenever $n_r > 1$, we have $|r_r| < 1$ and the expression for r in Eq. (3.6) converges absolutely. Fig. 4 shows σ for the single film system with a mirror behind. The solid line is the exact expression for σ, the dashed line is σ found by the ray model where only a few simple rays are included.

As shown in Fig. 4 very fast convergence is observed even if only a few of the shortest rays are included. The figure also shows that considering only the five simplest rays in the system, the analytically calculated absorption cross section can already be predicted near perfectly. Fig. 4 illustrates another important aspect, namely that our ray theory can describe absorption of electromagnetic radiation by including a complex refractive index.

4. Exact ray theory for multilayered films: hierarchical summation scheme

When a system has more than one layer, each ray, upon encountering a vacuum-film boundary or a boundary between two layers, will split into two rays, a reflected ray and a transmitted ray (except the mirror in our model system). This is called ray splitting [40–42]. With increasing geometric length, tracking splitting rays becomes an ever more complex task since each split ray, subsequently, will undergo splittings itself. Thus, the number of rays in the system increases exponentially with the number of splittings, i.e., with the geometric lengths of the rays.

In order to keep track of all the rays, we present a convenient bookkeeping system, called symbolic dynamics [43]. This system is widely used in the fields of non-linear dynamics and chaos. This symbolic language consists of an alphabet and simple grammatical rules which determine the path of a ray unambiguously. The symbolic dynamics of two film layers with a backside mirror (Fig. 5) has an alphabet that consists of the three letters (symbols) *a*, *b*, *c*. Each of the letters corresponds to a boundary where the ray will either split or simply reflect. The grammatical rules are:

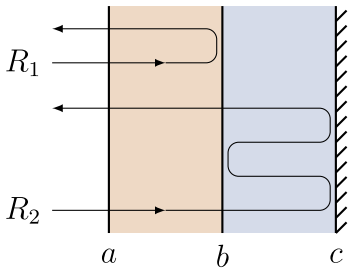

Fig. 5. Two rays, R_1 and R_2, in a system with a mirror and two film layers. R_1 and R_2 are labeled by the symbolic dynamics *aba* and *abcbcba*, respectively.

1. A word must start with the letter *a*. If the ray exits the system, the word must also end in the letter *a*.
2. Skipping letters is not allowed, i.e., unless the trajectory terminates, the letter *a* is always followed by the letter *b*, the letter *b* is always followed by letters *a* or *c* and the letter *c* is always followed by the letter *b*, indicating reflection off of the mirror.

Illustrating these rules, we construct the two sample rays R_1 and R_2 shown in Fig. 5. R_1 transmits at *a* and reflects at *b* before transmitting out of the system through *a*. Thus, the word labeling R_1 is *aba*. We may be tempted to label R_2 as *aca*, but this violates rule 2. The correct word, *abcbcba*, contains information about every boundary crossed.

To define the symbolic dynamics of systems with more films, we simply use a larger alphabet. If there is no mirror, i.e., transmission through the system is possible, rule 1 would allow words to end with the last letter of the alphabet.

The graph in Fig. 6 generates the part of the vocabulary that contains words with seven or less symbols for the two-film system in Fig. 5. The incoming ray will first hit node *a*. All *a* nodes are colored blue to emphasize that they mark the end of a word. The edges that are connecting the nodes are either black or red. A black edge signifies a ray traveling to the right and a red edge signifies a ray traveling to the left. A word can easily be read off Fig. 6 by writing down the successive letters starting from the first node to another blue node.

The computer implementation of this hierarchical summation scheme uses the number of ray splittings at the boundaries as a measure of the run time, not the number of rays explicitly. More splitting events generate exponentially more rays to approximate the reflectance R. About seven such splittings are needed to approximate the analytic expression reasonably well as seen in Fig. 7. These seven splittings generate a set of 64 contributing rays. Allowing more splittings, thus adding more rays, improves the approximation further.

If photons were classical, Newtonian particles, ray-splitting would not occur. The only ray allowed according to Newtonian mechanics would be the ray labeled *abcba*. Accordingly, this ray is also known as the “Newtonian ray” [44]. All other rays show ray splitting [40–42]. Since ray splitting is not allowed according to Newtonian mechanics, these split rays are called “non-Newtonian” [44]. Non-Newtonian rays have been proven theoretically [40,41,45,46] and experimentally [42,47–49].

To assess the importance of the (Newtonian forbidden) non-Newtonian rays compared with the (Newtonian allowed) non-split, Newtonian ray, we also show the contribution of the Newtonian ray to $R(\lambda)$ in Fig. 7. We see that the Newtonian ray alone, although in the vicinity of the exact result for $R(\lambda)$, produces a result with very poor accuracy. Conversely, Fig. 7 shows that the contribution of the split, non-Newtonian rays is substantial, and that only the added contribution of the split, non-Newtonian rays produces accurate results.

5. Importance of the correct summation order

As discussed in the previous section, in the case of a single film, the sum in Eq. (3.6) for the reflection amplitude r is absolutely convergent,

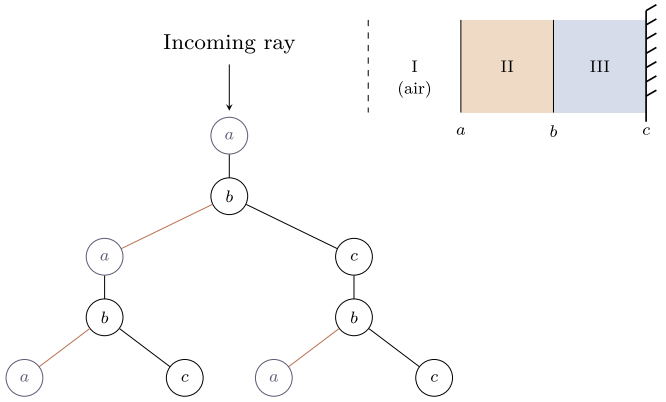

Fig. 6. Schematic of the ray tree algorithm. The interfaces between the materials II and III are labeled *a* and *b*, respectively, and the mirror is labeled *c*. An incoming ray always hits *a* first. At *a* the ray will split in two. One ray is reflected (ray labeled '*a*') and the other will travel to the right (black edge) towards *b*. At *b* it can either go to the left (red edge) and exit, or continue to travel to the right to the mirror, *c*. The inset shows the two-layered system that is considered in this example. (For interpretation of the references to color in this figure legend, the reader is referred to the Web version of this article.)

and the summation order of the rays is irrelevant. Any summation scheme, as long as all rays are included, will yield the exact value for r. However, if there is more than one film, the order of summation does matter. Let

$$r = \sum_{j=0}^{\infty} A_j \tag{5.1}$$

be the ray representation of the reflection amplitude. If Eq. (5.1) were a finite sum, the order in which we sum the rays would clearly not matter. However, this is not the case with infinite sums, such as Eq. (5.1). Only if

$$\sum_{j=0}^{\infty} |A_j| < \infty \tag{5.2}$$

is the summation order of the terms in Eq. (5.1) irrelevant and always yields the correct reflection amplitude. In this case, as discussed in the previous section, we call the sum in Eq. (5.1) absolutely convergent. If, however,

$$\sum_{j=0}^{\infty} |A_j| = \infty, \tag{5.3}$$

it was shown by Riemann [50] that, depending on the summation order of the terms in Eq. (5.1), the infinite sum in Eq. (5.1) can be made to have any prescribed value. This is known as Riemann's Rearrangement Theorem [51]. In this case the sum in Eq. (5.1) is called conditionally convergent, and it is necessary to sum it in some prescribed way in order to obtain correct results.

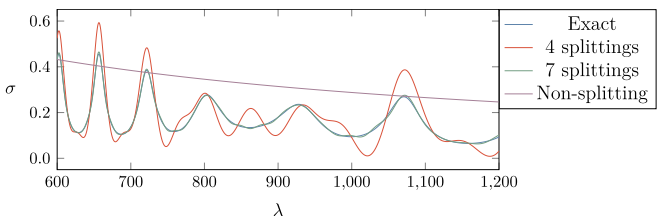

Fig. 7. Absorption cross section σ as a function of the wavelength λ, including various numbers of split rays, and the shortest non-splitting ray. The hierarchical summation scheme approximates the analytical result for the film with two layers (Fig. 5) almost perfectly with only 64 rays or, equivalently, seven splittings. Including more rays yields an even more accurate result. The non-splitting ray approximately defines the lower envelope of the exact result.

In Appendix D we show that for our two-film system, for a large range of dielectric constants, Eq. (5.3) holds, i.e., in these cases our ray sum in Eq. (5.1) is only conditionally convergent. The correct summation scheme in these cases is to sum the rays in the order of increasing path length, where the path length of the ray may either be its geometric length or its optical path length. This summation scheme is not dictated by mathematics, which does not help us beyond the fact of stating that in the case of conditional convergence different summation prescriptions produce different results [51], but interestingly is dictated by the physical situation. For actual realizations of solar cells there is always some absorption present, which naturally suppresses the importance of longer rays. Therefore, ordering the rays according to their importance for r means ordering them according to their path lengths.

We can numerically corroborate the importance of the summation order by testing for absolute convergence with the hierarchical summation scheme. We take the absolute value of each term, which is equivalent to removing the phase completely. Fig. 8 compares the absolute value of the difference between the analytical reflection probability R_A and the reflection probability R_{HSS}, computed according to the hierarchical summation scheme. Without the absolute value of each term, i.e., when phases are included, convergence is reached after a small number of splittings. Without phases, we see that the difference $|R_A - R_{HSS}|$ is diverging, numerically corroborating that the sum over rays is not absolutely convergent.

6. Importance of phases in the ray theory

In this section we emphasize the importance of phases, even in the case of absorption (which was not included in Sec. 5), by computing absorption cross sections, with and without phases included, using as an example the single film with mirror introduced in Secs. 2 and 3. Comparing the two cases, we show that the ray theory without phases produces results that contain unacceptably large errors.

In order to demonstrate the importance of the phases, we introduce the following ray model where phases are not included. Without phases, instead of being associated with an amplitude, every ray is associated with an intensity. We set the incoming intensity of the ray to I_0. The simplest ray model we consider retains only the directly reflected ray as illustrated in Fig. 3a. We call this ray *the ray of zero length*, since it does not enter the energy-converting film, and its optical path length inside of the film, therefore, is zero. We further assume that the probability given in Eq. (2.1) describes the amount of light reflected at the surface of the film. The rest of the light is absorbed in the film. In this case the absorption depends on the wavelength of the incoming light only through the wave number, k, as long as the refractive index of the film is constant for all wavelengths. When we evaluate rays that travel inside of the film, the intensity assigned to a particular ray decreases via Beer-Lambert's Law, and is expressed as

$$I = I_0 e^{-n_i k x}, \tag{6.1}$$

where I_0 is the incoming intensity of the light, which we set to 1, x is the distance travelled in the film [39,52], k is the wave number and n_i is the imaginary part of the refractive index of the film.

To find the amount of absorbed light, i.e., the absorption cross section, σ, we need to sum the contributions to the absorption from each ray. When the ray hit a boundary, a part of it will reflect and a part of it will transmit. The probability for reflection at a boundary, R_b is given in eq. (2.1) and the probability of transmission is $T_b = 1 - R_b$. Evaluating σ due to the rays in Fig. 3a and b, the result is

$$\sigma = 1 - \left(R_b + T_b^2 e^{-2n_i k a}\right), \tag{6.2}$$

where a is the width of the film. The expression inside the brackets is the sum of the intensities of these two reflected rays. When all possible rays are included (infinitely many), σ is given by

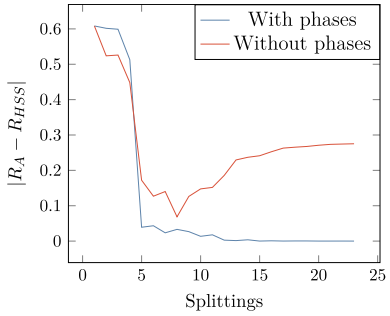

Fig. 8. Absolute value of the difference between the reflection calculated by the analytical expression, R_A, and the hierarchical summation scheme, R_{HSS}, is converging when the phase of the rays is included. The same calculation will diverge if it is done without phases.

$$\sigma = 1 - \left(R_b + \frac{T_b^2 e^{-2n_l ka}}{1 - R_b e^{-2n_l ka}} \right). \tag{6.3}$$

We arrive at this formula by summing up all possible rays and by using the elementary summation formula for the geometric series.

Fig. 9 shows a comparison of the absorption cross section evaluated with ray models that include and neglect phases, respectively. For the case in which phases are neglected, we present three different scenarios. (1) The horizontal blue line in Fig. 9 is σ computed by including only the ray of zero length (see Fig. 3a). (2) The red line in Fig. 9 is σ computed on the basis of the two rays in Fig. 3a and b (Eq. (6.2)). (3) The green line in Fig. 9 is σ obtained by including infinitely many rays (Eq. (6.3)). Contrasting these three cases, computed without including phases, we also show the exact result for σ in Fig. 9, where we have included infinitely many rays *with phases* (purple line). The exact result, with phases included, shows oscillations (purple line), which are not captured by either of the three cases that do not include phases. As seen in Fig. 9, σ without phases is monotonically decreasing when the wavelength increases (green and red lines), without any oscillations according to Eq. (6.1). The result without phases included underestimates the exact result with phases included, and, according to Fig. 9, the relative error can exceed 60% in the wavelength region shown in Fig. 9. In the context of absorption cross sections of typical solar cells, an error of this magnitude is not acceptable. We conclude that for accurate modelling of solar-cell efficiencies in terms of rays, inclusion of phases is absolutely essential. Any ray theory, whether applied in the electromagnetic, acoustic, or quantum domains, is exact only if phases are

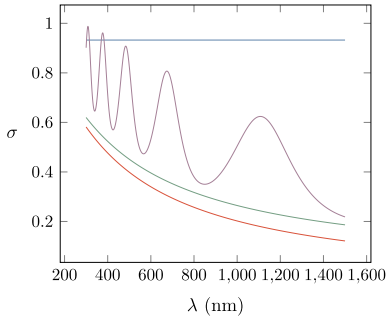

Fig. 9. Absorption cross section, σ, as a function of wavelength,λ, in the range 300 nm $\leq \lambda \leq$ 1500 nm, for a single film with refractive index $n = 1.8 + 0.05i$, a thickness of 500 nm, and a mirror on the backside of the film. The blue line is σ, including only the reflected ray of zeroth length (see Fig. 3a). The red line is σ, including only the two simplest rays (see Fig. 3a and b, calculated with Eq. (6.2). The green line is σ, including infinitely many rays without phases, calculated with Eq. (6.3), and the purple line is σ, including infinitely many rays with phases. The purple line is calculated with the ray theory presented in Sec. 3. (For interpretation of the references to color in this figure legend, the reader is referred to the Web version of this article.)

included. Neglecting phases may have serious consequences, ranging from incorrect results to divergent results as demonstrated in Fig. 8 of Sec. 5.

7. Signatures of rays in the Fourier transform of the reflection amplitude

A Fourier transform of the reflection amplitude $r(k)$ allows us to reveal the signatures of the rays whose combined contributions result in the exact functional form of $r(k)$. If the entire spectral range is accessible to us, we obtain this information in the form of the *length spectrum*

$$\mathscr{F}(L) = \frac{1}{2\pi} \int_{-\infty}^{\infty} r(k) e^{-iLk}\, dk. \tag{7.1}$$

To illustrate, let us use the exact, explicit formula 3.6 for the reflection amplitude r of a single film with mirror. We obtain

$$\mathscr{F}(L) = r_l \delta(L) + \frac{t_l t_r}{r_r} \sum_{\nu=1}^{\infty} e^{i\nu\pi} r_r^{\nu} \delta(L - 2na\nu), \tag{7.2}$$

where $\delta(x)$ is Dirac's delta function. We see that $\mathscr{F}(L)$ is a series of sharp peaks at integer multiples of the optical path length $2na$, where each peak corresponds to the optical path length of a certain ray inside of the film. Thus, every single ray that contributes to Eq. (3.6) is represented as a sharp peak in $\mathscr{F}(L)$. This even includes the "ray of zero length", which is the ray that reflects with amplitude r_l off of the front surface of the film. Since this ray does not enter the film, its optical path length in $\mathscr{F}(L)$, naturally, is zero. The weights of the δ terms in Eq. (7.2) correspond to the amplitudes that the rays pick up when crossing a boundary or being reflected from a boundary. Thus, the length spectrum of r contains the complete optical information of the system under consideration. This is not surprising, since the Fourier transform in Eq. (7.1), a function in L space, is complementary to the ray representation, Eq. (3.6), of r in k space. Unfortunately, ray information can be extracted so cleanly from $r(k)$ with Eq. (7.1) only if the integration range is infinite. In actual applications in solar cells, we are restricted to a finite spectral range, which turns the exact length spectrum $\mathscr{F}(L)$ into an approximate length spectrum

$$\widetilde{\mathscr{F}}(L) = \frac{1}{2\pi} \int_{k_1}^{k_2} r(k) e^{-ikL}\, dk. \tag{7.3}$$

Applied to our single-film example, this evaluates to

$$\begin{aligned} \widetilde{\mathscr{F}}(L) \;=\; & \tfrac{r_l}{2\pi} \exp\left[-i\left(\tfrac{k_1+k_2}{2}\right)L \right](k_2 - k_1)\, \mathrm{sinc}\left[\tfrac{L}{2}(k_2 - k_1) \right] \\ & + \tfrac{t_l t_r}{2\pi r_r}(k_2 - k_1) \textstyle\sum_{\nu=1}^{\infty} e^{i\nu\pi} r_r^{\nu} \exp\left[i\left(\tfrac{2na\nu - L}{2}\right)(k_1 + k_2) \right] \\ & \times \mathrm{sinc}\left[\left(\tfrac{2na\nu - L}{2}\right)(k_2 - k_1) \right], \end{aligned} \tag{7.4}$$

where $\mathrm{sinc}(x) = \sin(x)/x$ is the "sinc-function". We see that in the case of a finite spectral range the sharp δ-function peaks are replaced by smooth, oscillatory sinc-functions, which produces "Gibbs ringing" [53] in $\widetilde{\mathscr{F}}(L)$ that produces copious "extra peaks" in $\widetilde{\mathscr{F}}(L)$ and may thus obscure the peaks that correspond to rays. The ringing may be reduced by the use of a window function [54], i.e., a function $w(k)$ that softly "switches on" and "switches off" the integration at k_1 and k_2 according to $w(k_1) = w(k_2) = 0$, $w'(k_1) = w'(k_2) = 0$, $w''(k_1)/k_1^2 \ll 1$, $w''(k_2)/k_2^2 \ll 1$.

As an illustrative example we present the Fourier transform of the reflection amplitude of a three-layered film with constant, non-dispersive indices of refraction, $n_1 = 1.5$, $n_2 = 1.9$, $n_3 = 2.3$, and film widths $a_1 = 500$ nm, $a_2 = 2000$ nm, and $a_3 = 1000$ nm, respectively. In this example we chose $k_1 = 2\pi/1200$ nm and $k_2 = 2\pi/5$ nm. We used the window function

$$w(m) = 1 - \left(\frac{m - \frac{N-1}{2}}{\frac{N-1}{2}} \right)^2, \tag{7.5}$$

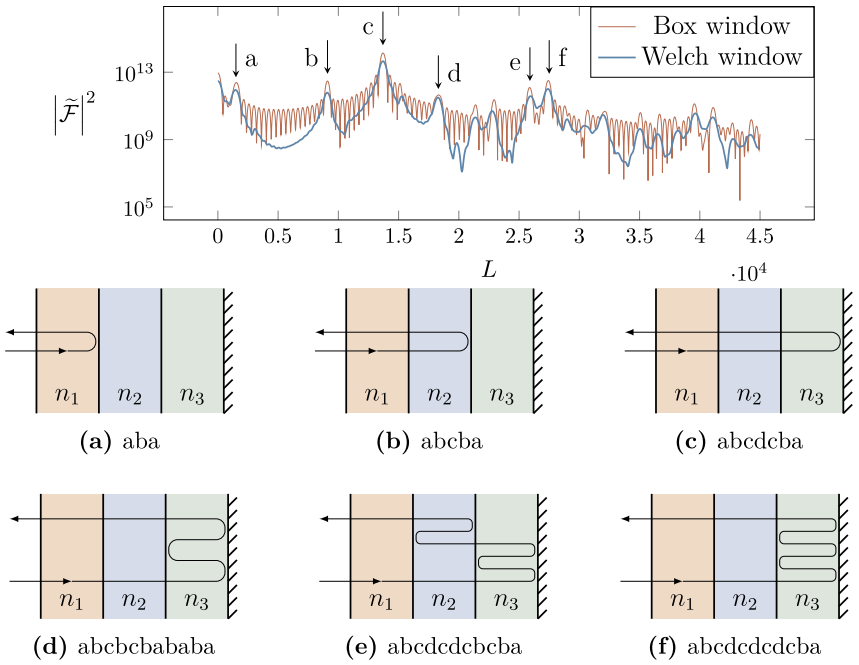

Fig. 10. Top frame: Finite-range Fourier transform (approximate length spectrum) $\widetilde{\mathcal{F}}(L)$ of the exact $r(k)$ of a three-layer film system with mirror with parameters as specified in the text. $\widetilde{\mathcal{F}}(L)$ shows distinct peaks, labeled (a)–(f). The rays corresponding to these peaks, including their symbolic-dynamics labels, are illustrated in the six frames (a)–(f), below the top frame, respectively. These six rays make the most important contributions in the ray-representation of $r(k)$ of this system.

called the Welch window function. Here m is an integer variable that corresponds to the grid used in the calculations. If we are using M different values of k, m takes the values $0 \le m \le M-1$. Using no window (box window) shows Gibbs phenomenon very clearly. The resulting length spectrum of this three-layer system is displayed in Fig. 10. In general, a larger Fourier peak indicates a more important component in a Fourier series. Hence, the heights of the peaks in Fig. 10 directly relate to the importance of the contributions of the corresponding rays to r. The peaks labeled a-f in Fig. 10 correspond to the rays illustrated in (a) - (f) of Fig. 10, respectively. The six tallest peaks correspond to rays labeled by the words *aba*, *abcba*, *abcdcba*, *abcbcbababa*, *abcdcdcbcba*, and *abcdcdcdcdcba*, respectively. The peaks in Fig. 10 are located at the optical path lengths of the rays, i.e., they are located at the linear combinations $2\nu_1 n_1 a_1 + 2\nu_2 n_2 a_2 + 2\nu_3 n_3 a_3$, where ν_j, n_j, and a_j are the repetition number, index of refraction, and width of layer number j, respectively.

As shown in this section, whenever we have $r(k)$, either analytically or numerically calculated, or experimentally determined, a Fourier transform of $r(k)$ reveals the peaks of the corresponding multi-layer system, a technique we call *ray spectroscopy*. The peak heights will tell us which of the rays are the most important in determining the reflection amplitude r, which, in turn, determines the absorption cross section of the corresponding solar cell. As shown in Fig. 10, the peak height is an exponentially decreasing function of optical path length, which means that only a few of the shortest rays are necessary to determine $r(k)$ with sufficient accuracy to be useful for system optimization. This, in turn, enables us to design and optimize solar cells in a completely new way on the basis of a few important rays, which implies a very small parameter space to be searched for system optimization.

8. Example with silicon

To provide an example of the ray-wave equivalence and the hierarchical summation scheme, we analyzed a three-layer simplification of a five-layer optically thin, epitaxial crystalline silicon solar cell using experimentally determined indices of refraction [55–58]. Fig. 11 shows the layer structure for these two models. The intent with the simple three-layer design is to demonstrate the concepts described in this paper applied to a system with material constants of practical importance. However, it should be noted that solar cells with co-planar structure are mainly used to provide an example. Commercial solar cells usually have some kind of surface structure to lower the reflectivity.

Since both the two amorphous silicon (a-Si) layers and the two crystalline silicon (c-Si) layers in the experimentally realized solar cell

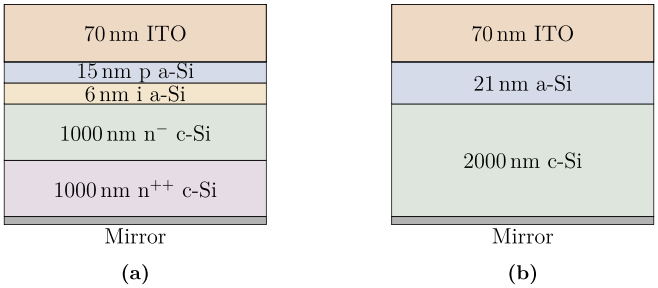

Fig. 11. Multilayer solar cells with mirror. (a) Experimentally realized thin epitaxial crystalline silicon solar cell consisting of five layers [55]. (b) Three-layer simplified model of the experimental system shown in (a), obtained by replacing layers with different doping but approximately the same index of refraction by a single layer. The three layers are, from top to bottom, 70 nm ITO, 21 nm amorphous silicon, and 2000 nm intrinsic silicon, respectively.

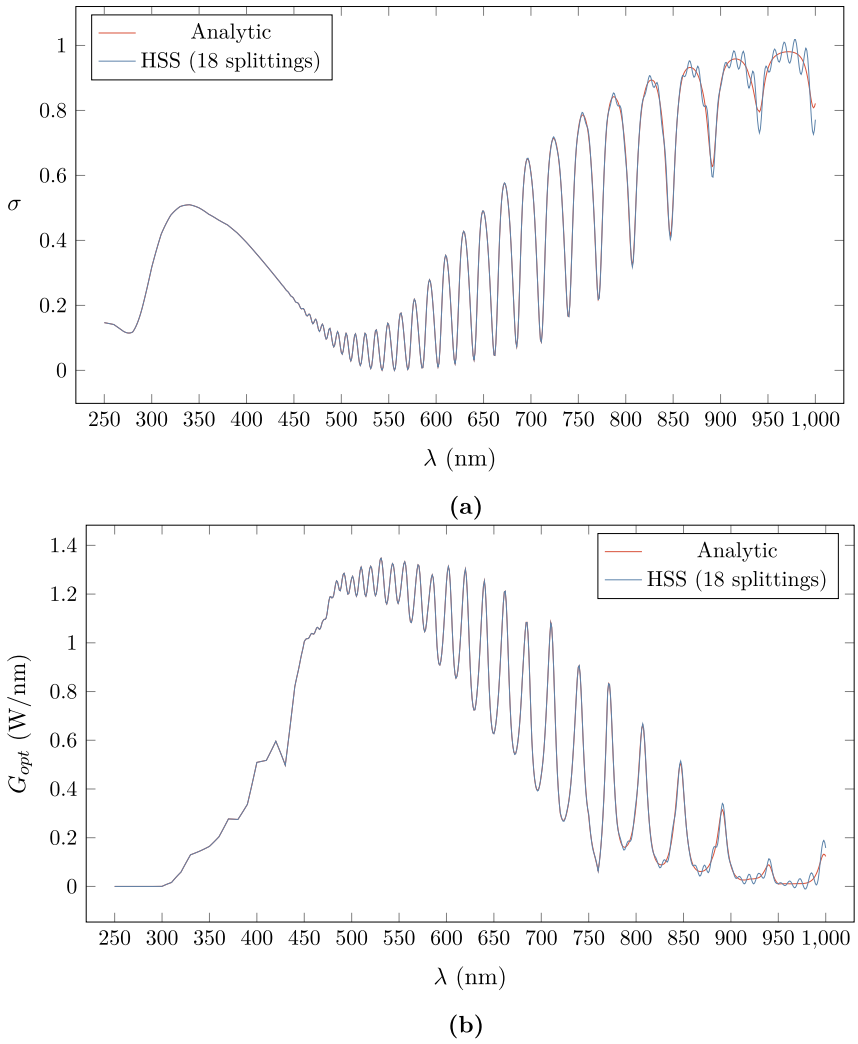

Fig. 12. a) A comparison of the absorption cross section σ calculated from an analytic expression and with a finite number of rays, using the hierarchical summation scheme (HSS). 18 splittings produce 65,537 rays and gives a good approximation to the analytic expression. b) When the AM1.5 solar spectrum [59] is taken into account, we get the optical generation rate, G_{opt}.

differ only in their doping, and since we for now neglect the doping-dependent free carrier absorption, we modeled this solar cell in terms of a three-layer system by collapsing the two a-Si layers and the two c-Si layers into a single layer, respectively.

Fig. 12a shows a comparison between the analytical result (red line) for the absorption cross section σ and the result produced by the hierarchical summation scheme (blue line). In the lower wavelength regime, σ is perfectly approximated by the hierarchical summation scheme including 18 splittings or 65,537 rays. Only from 750 nm on do we start to see some deviations. This demonstrates the complexity of a three-layer film in terms of its ray dynamics, and highlights the power of the hierarchical summation scheme even in the case of dispersive indices of refraction.

In order to obtain the optical generation rate [59], Eq. (2.5), we multiply σ with the AM1.5 solar spectrum, Γ. The result is displayed in Fig. 12b for both the analytical expression (red line) and the hierarchical summation scheme (blue line), corresponding to the two corresponding cases shown in Fig. 12a, respectively.

Once more, we see excellent agreement between optical generation rate obtained on the basis of the analytical and hierarchical summation scheme results.

9. Discussion

As shown in section 3, there is a profound duality between waves and rays. Rays are governed by ordinary differential equations, describing particle motion, while wave fronts are the solutions of continuous wave equations expressed in the language of partial differential equations. This duality is exploited in many fields of physics that deal with waves. In optics, e.g., it leads to the important field of geometric optics [60] in which one attempts to obtain an accurate description of the passage of light through various optical components by using a ray picture, side-stepping the more involved solution of Maxwell's wave equations [39,61]. There are many examples where the wave-ray duality is exact (see, e.g., [30]) and may be exploited to advantage. The most important example is Feynman's path integrals [62], which solve the full wave-mechanical problem of quantum mechanics exactly by summing over all possible classical rays. Another example of exact ray solutions to the corresponding wave problem is quantum mechanics with energy-scaling step potentials in one dimension [63–65]. Since the quantum step-potential problem and the electromagnetic (E&M) optically thin solar-cell problem are formally identical problems, one of the intentions of this paper is to transfer and adapt methodology from the quantum chaos community in the field of one-dimensional energy-scaling step potentials and dressed quantum graphs [64,65] to the solar-

cell community, who is concerned with the solution of Maxwell's equations for stacks of layers of anti-reflection coatings on top of energy-converting materials. We note that, so far, only the bound-state problem has been studied extensively in the context of dressed, scaling quantum graphs, which, in the optical case, would correspond to the presence of two mirrors, one at the front and one at the back of the stack of films. The scattering problem, as studied in this paper, has to our knowledge not yet been studied in the context of dressed, scaling quantum graphs.

For the one-dimensional case we derived the exact expression for the *absorption cross section*, σ, of the energy-converting material. When σ is weighed by the solar spectrum as the spectral weighting term, the *optical generation rate* is obtained. This brings out the connection between the structure of the wave function ψ and the absorption. By evaluating σ we can engineer our system to increase the absorption, and thus the absorption cross section, of the system.

We showed the importance of including phases in our ray theory with the help of the following two-step method. First, we include the exact phases of the rays in our one-dimensional model, which we take as consisting of a single film. In section 3 we demonstrate that this yields the exact solution of the Helmholtz equation. Then, we evaluated the ray sum for this one-dimensional systems setting all phases to 1. We showed in Section 5 that the resulting, incorrect ray theory cannot handle the resonances and in addition predicts a spectral optical generation rate that is up to 60% off. We are convinced that this observation carries over to any ray tracing in two and three dimensions, which means that in order to be confident in the accuracy of a ray-tracing result, phases *must* be included. Otherwise, as shown in our paper in the one-dimensional case, one should be prepared for large errors in the predictions of a ray theory that omits phases.

For several of our model systems, including our example of the lab silicon cell discussed in section 8, we showed that including only a few rays in the ray sum already gives a good approximation of the absorption cross section (see, e.g., Fig. 4. This observation is important since, in principle, an infinity of rays needs to be summed over in order to obtain exact results, and if the convergence were slow, this would result in an enormous number of terms to be summed, partially, or totally, cancelling out the advantage in computational speed of rays over waves. That only a few dominant rays already determine the final result with good accuracy is particularly important in two and three dimensions, since, according to the increased dimension, the set of rays that needs to be summed over is much larger.

Since our ray theory is exact, it works for all refractive indices, n. This includes all n typically encountered in solar cells, where complex n indicates an absorptive material. A strength of the ray theory is that the refractive index can have any value and is not limited to only small values of real and imaginary parts. Our ray theory is therefore applicable to any solar cell material. Including the temperature dependence of its index of refraction. In linear approximation, as a function of temperature T, we can write

$$n(T) = n_0(T_0) + \beta(T - T_0), \tag{9.1}$$

where n_0 is the complex index of refraction at a reference temperature T_0 and β is the complex temperature coefficient, combining the two temperature coefficients for the real and imaginary parts of the index of refraction. Since our theory is exact for all indices of refraction, our theory can accommodate exactly the temperature dependence of the index of refraction, described by the temperature coefficients. In addition, since our complex index of refraction models the effects of the band gap and any gain and loss mechanisms, their temperature dependence, via the complex index of refraction, is included as well. We would also like to point out here that complex indices of refraction have so far not been treated in the quantum ray-splitting literature. Therefore our paper is the first to show that a complex index of refraction does not invalidate the exactness of the ray theory.

In our theory the boundary conditions between the vacuum and dielectric films, and between different dielectric films, are treated exactly, without any approximations. Only the boundary condition between the energy-converting dielectric film and the mirror is idealized, assuming 100% reflection. This assumption is not necessary since the mirror can be treated as another dielectric layer [39] for which our theory is exact.

Two-dimensional materials are of great current interest (see, e.g., [66,67]). Since the dielectric properties of these materials have already been measured [68], reflection and transmission amplitudes of these two-dimensional materials can be computed. Once these amplitudes are known, our theory is applicable to these materials and stays exact.

We do not hesitate to point out that for one-dimensional systems wave calculations are cheaper than ray calculations. For one-dimensional multi-layer systems, the transfer matrix method [69] can be used, which is fast and includes absorption. Even in two dimensions, solving the wave equation might still be cheaper and faster than applying the ray theory. In three dimensions, however, supported by the fact that an extensive literature on ray-tracing in three dimensions exists [15,16,27,28], we believed that ray methods will have an edge, in particular when constructed with phases included, which renders them exact.

In addition to paving the way toward an exact and efficient ray theory in three dimensions, the emphasis of this work is to present a ray theory that can be used to understand the different mechanisms that may be used to improve the absorption cross section. The fact that only a few rays describe the absorption cross section, σ, of the system is encouraging since only a few parameters (rays) need to be optimized for optimizing the entire system. Consequently, there are two ways in which classical ray calculations can be used in the context of solar cells: (1) As a predictive tool used to predict the outcomes of wave calculations (predictive direction; forward model) and (2) as a means to understand the results of wave calculations, in particular to illuminate and illustrate the mechanisms by which enhancement of the absorption cross section is achieved (analysis direction).

In the case of a single film, we showed in section 5 that the ray sum is absolutely convergent. Therefore, the terms in the sum may be summed in any order. In the case of stacks of two or more films, however, we showed in section 5 that the resulting ray sum is only conditionally convergent. In this case the order of summation is important, since, according to Riemann [50,70], any result can be obtained from a conditionally convergent sum by cleverly re-ordering the terms. In section 4 we present a hierarchical scheme according to which the rays in a multi-layer system can be summed in correct order.

The dominant rays describing the system can be found by performing the Fourier transform of σ, Thus, the Fourier transform provides us with the possibility of extracting ray information from σ. It is important to use a windowed Fourier transform (requiring a switching function) to eliminate the Gibbs ringing, which produces spurious peaks in the Fourier transform that do not correspond to rays. We found that rays are connected to the absorption cross section. The longer the rays, the larger the absorption cross section. The Fourier transform gives us the ability to study the dominant rays. By increasing the dominance of the long rays, which have the largest contribution to the absorption, it is possible to design solar cells to have an increased absorption cross section.

In section 8 we study a realistic system with a refractive index that exhibits dispersion. We showed at even dispersion is no obstacle to our theory; it still provides us with the correct absorption cross section.

Sunlight is incoherent and the question arises whether our results, derived for coherent light, are relevant for illumination of solar cells with incoherent light. We answer this question in the affirmative, since what we evaluate is the absorption cross section, which is defined for a sharp frequency, associated with an infinite coherence length. Another way to see this is the following. On the microscopic level, it is individual photons that strike the solar cell and interact with it. While different photons certainly have different frequencies, each individual

photon has a sharp frequency and a corresponding wave function that is the solution of the optical Helmholtz equation. Thus, at each individual frequency, it is indeed the Helmholtz equation that governs the absorption of photons and thus determines the absorption cross section. The total optical generation rate is then obtained by a simple integral over the absorption cross sections weighted with the solar spectrum. Thus, our theory, despite the fact that sun light is incoherent, works for all film thicknesses.

10. Conclusions

In this paper we have shown that the ray theory is exact in one dimension. Our results are important since they pave the way to the use of exact ray tracing in three dimensions, which allows for both including textures and other scattering surfaces, as well as oblique incidences of sunlight.

We also showed several other facts that are important for the extension of the ray theory to three dimensions. We showed that the summation order of the rays is important and that it is dangerous, although tempting, to sum sub classes of rays to infinity, and then add the sub classes results. We showed explicitly that this will yield incorrect results.

An important result we obtained is that phases must be properly computed and included with each ray that is used to compute reflection probabilities and the absorption cross section. Without including the phases, as is sometimes done in current three-dimensional Monte-Carlo simulations of ray tracing in solar cells, we showed that an error of up to 60% and larger can be incurred.

We also showed that including only a few rays in the sum over rays gives quite accurate results, provided the phases are also correctly included. This is of the utmost importance for three-dimensional applications since, as a consequence of ray splitting, as we showed in Section 5, the number of rays explodes exponentially in the lengths of the rays that need to be included to obtain converged results with acceptable accuracy. We also showed that the rays are "real" in the sense that their signatures can readily be seen in the Fourier transform of the reflection probability as peaks in the length spectrum.

Since our theory is exact, it works for all refractive indices n, even if n is complex, which includes indices of refraction typical for solar cell materials. We showed this explicitly in Section 8, where we discuss the application of our exact ray theory to an example of a silicon solar cell. Extension of our theory to two and three dimensions is straightforward and provides the basis for future work on the application of exact ray theories for the computation of the absorption cross section of solar cells of practical importance.

Acknowledgement

This work was supported by the grant "Development of a new ray model for understanding the coupling between dielectric spheres for photovoltaics with higher efficiency" - No: 250678 financed by The Research Council of Norway.

The contributions from Maren Anna Brandsrud and Eivind Seim are considered to be equal, thus the first author and second author was decided by alphabetical order.

Appendix A. Reflection and transmission amplitudes

In order derive the exact ray model, we need to include the phases. The phases are described as below:

To obtain the proper phases for reflection and transmission of a ray at the left edge of a material, we consider the potential shown in Fig. A.1.

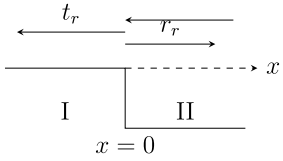

Fig. A.1. When a ray is coming from the left and goes from region I (vacuum) to region II (material with refractive index n), the ray will split into a transmitted and a reflected ray at the boundary. The amplitudes of this rays are given by the reflection and transmission amplitudes, r_l and t_l.

Coming from the left, out of region I ($x < 0$), a ray encounters the left edge of region II at $x = 0$. It gets reflected back into region I with reflection amplitude r_l, and gets transmitted into region II with amplitude t_l. The subscript l stands for "left". In region I it is vacuum. In order to find the correct phase of the amplitude, we need to use the wavenumber of the corresponding wave and k is given by $\frac{2\pi}{\lambda}$, where λ is the wavelength. In region II, the wavenumber of the corresponding wave is given by $k_{II} = nk$ where n is the refractive index in region II. The wavefunction in region I and II are:

$$\Psi_I = e^{ikx} + \eta e^{-ikx}, \tag{A.1}$$

$$\Psi_{II} = t_l e^{ik_{II}x}. \tag{A.2}$$

Using the continuity of the wavefunction and its first derivative at $x = 0$, we obtain:

$$\eta = \frac{1-n}{1+n}, \tag{A.3}$$

$$t_l = \frac{2}{1+n}. \tag{A.4}$$

When the wave is coming from the right, the ray will encounter the boundary as shown in Fig. A.2.

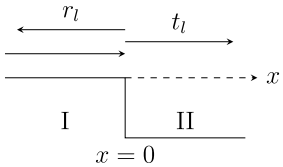

Fig. A.2. Reflection and transmission amplitudes, r_r and t_r, respectively, for a ray incident from the right (out of region II, i.e., $x > 0$).

The wavefunctions are

$$\Psi_I = t_r e^{-ikx}, \tag{A.5}$$

$$\Psi_{II} = e^{-ik_{II}x} + r_r e^{ik_{II}x}. \tag{A.6}$$

Again using continuity and the continuity of the first derivative gives us

$$r_r = -\left(\frac{1-n}{1+n}\right), \tag{A.7}$$

$$t_r = \frac{2n}{1+n}. \tag{A.8}$$

Appendix B. Integral formula for the spectral optical generation rate

In the scalar one-dimensional theory, the radiative flux, up to a constant, is defined by

$$j = \frac{1}{2i}\left(\psi^* \frac{d}{dx}\psi - \psi \frac{d}{dx}\psi^*\right). \tag{B.1}$$

Since, according to Fig. 1, the incident radiation is described by the plane wave $\psi_{in} = e^{ikx}$, the flux of the incident radiation is

$$j_{in} = \frac{1}{2i}\left(e^{-ikx}\frac{d}{dx}e^{ikx} - e^{ikx}\frac{d}{dx}e^{-ikx}\right) = k > 0. \tag{B.2}$$

Since, according to Fig. 1 the reflected radiation is described by $\psi_{refl} = re^{-ikx}$, a calculation analogous to Eq. (B.2) yields

$$j_{refl} = -|r|^2 k = -Rk < 0. \tag{B.3}$$

The total flux on the left-hand side of the boundary is thus

$$j = j_{in} + j_{refl} = k - Rk. \tag{B.4}$$

In terms of flux, the reflection probability R is defined as

$$R = \left|\frac{j_{refl}}{j_{in}}\right| = |r|^2, \tag{B.5}$$

which is consistent with our earlier definition Eq. (2.1) of the reflection probability above. We now turn to the wave equation, i.e.,

$$\frac{d^2\psi}{dx^2} = -n^2k^2\psi. \tag{B.6}$$

Taking the complex conjugate, we arrive at

$$\frac{d^2\psi^*}{dx^2} = -(n^2)^*k^2\psi^*. \tag{B.7}$$

From Eqs. (B.6) and (B.7) we obtain

$$\psi^*\frac{d^2\psi}{dx^2} - \psi\frac{d^2\psi^*}{dx^2} = [(n^*)^2 - n^2]k^2|\psi|^2. \tag{B.8}$$

We can also write the left-hand side of Eq. (B.8) as

$$\psi^*\frac{d^2\psi}{dx^2} - \psi\frac{d^2\psi^*}{dx^2} = \frac{d}{dx}\left[\psi^*\frac{d\psi}{dx} - \psi\frac{d\psi^*}{dx}\right] = 2i\frac{d}{dx}j(x), \tag{B.9}$$

where we used equation Eq. (B.1).

We now specialize to the situation shown in Fig. 2b, i.e., the film with mirror. For this situation, we now integrate Eq. (B.9) with Eq. (B.8) over the width of the film to obtain

$$\begin{aligned} 2i\int_0^a \tfrac{dj}{dx}dx &= 2i[j(a) - j(0)] \\ &= 2i[0 - k(1-R)] \\ &= \int_0^a [(n^*)^2 - n^2]k^2|\psi|^2 dx \\ &= \int_0^a (-4in_r n_i)k^2|\psi|^2 dx. \end{aligned} \tag{B.10}$$

Therefore, we now obtain

$$R = 1 - 2k\int_0^a n_i n_r |\psi|^2 dx \tag{B.11}$$

and

$$\sigma = 1 - R = 2k\int_0^a n_i n_r\ |\psi|^2 dx. \tag{B.12}$$

Appendix C. Equivalence of the 1-R with the spectral optical generation rate

In this appendix we demonstrate that the two different approaches presented in section 2 lead to the same formula for the absorption cross section σ. For a single film on a mirror (Fig. 2a) the wavefunction ψ inside the film is

$$\psi = \frac{-2\sin[nk(x-a)]}{\sin(nka) + in\cos(nka)}, \tag{C.1}$$

where a is the film thickness, n is the complex refractive index and k is the wavenumber. The absorption cross section is

$$\sigma = 2k\int_0^a |\psi|^2 n_i n_r dx. \tag{C.2}$$

This can also be written as

$$\sigma = 2kn_r n_i\left(\frac{2}{\eta^2+\theta^2}\right)\int_0^a \cosh[2n_i k(x-a)] - \cos[2n_r k(x-a)]dx, \tag{C.3}$$

where the prefactor contains

$$\begin{aligned}
\eta &= \gamma - n_i\varepsilon + n_r\zeta \\
\theta &= \delta + n_i\zeta + n_r\varepsilon \\
\gamma &= \sin(n_r ka)\cosh(n_i ka) \\
\delta &= i\cos(n_r ka)\sinh(n_i ka) \\
\varepsilon &= \cos(n_r ka)\cosh(n_i ka) \\
\zeta &= i\sin(n_r ka)\sinh(n_i ka).
\end{aligned} \tag{C.4}$$

Evaluation of the integral is straightforward and results in

$$\frac{2}{\eta^2+\theta^2}[n_r\sinh(2n_i ka) - n_i\sin(2n_r ka)]. \tag{C.5}$$

To complete our task, we have to show that $1-|r|^2$ from the scalar wave model produces the same result. The reflectivity $|r|^2$ is

$$|r|^2 = \left|-\frac{n\cos(nka) + i\sin(nka)}{n\cos(nka) - i\sin(nka)}\right|^2, \tag{C.6}$$

which can be rewritten as

$$|r|^2 = \frac{(n_r\varepsilon + n_i\zeta - \delta)^2 + (n_i\varepsilon - n_r\zeta + \gamma)^2}{\theta^2+\eta^2}. \tag{C.7}$$

Inserting this together with γ, δ, ε, and ζ into $1-|r|^2$ yields exactly the same result as in Eq. (C.5).

Appendix D. Proof of importance of the summation order

In this Appendix we show that for our two-film system and for a large range of dielectric constants, Eq. (5.3) holds, i.e., in these cases our ray sum in Eq. (5.1) is only conditionally convergent. We show this by observing that if the sum in Eq. (5.3) is already infinite for a subclass of rays, it is certainly infinite when summing over all rays, since all the terms not taken into account are positive. The subclass we focus on consists of rays that make p right reflections on the vacuum/film interface and make q right reflections on the film/film interface (see Fig. D.1). We also exclude any left reflections on the film/film interface, which uniquely defines our subclass of rays. Three examples of rays in our subclass are shown in Fig. D.1. All three rays have $p=1$ and $q=2$, and they contribute the same amplitude to r in Eq. (5.1). They differ only in their sequence of bounces. This induces degeneracy in our ray sum. In fact, any class of rays, characterized by a given p and q, is $\binom{p+q}{p}$ fold degenerate, where $\binom{p+q}{p}$ is the binomial coefficient [71]. The total contribution ρ of all of the rays of our subclass to the total reflection amplitude r is

$$\rho = \sum_{p=0}^{\infty}\sum_{q=0}^{\infty}\binom{p+q}{p} t_1^2 t_2^{2p+2} r_1^p r_2^q e^{ik[2(p+1)n_1a_1 + 2(p+q+1)n_2a_2]}, \tag{D.1}$$

where t_1 and r_1 are transmission amplitude and right-reflection amplitude at the vacuum/film interface, t_2 and r_2 are transmission amplitude and right-reflection amplitude at the film/film interface, a_1 is the width of film 1, a_2 is the width of film 2, and n_1 and n_2 are the refractive indices of films 1 and 2, respectively. To check whether the double sum in Eq. (D.1) is absolutely convergent, we need to check whether

$$\rho' = \sum_{p=0}^{\infty}\sum_{q=0}^{\infty}\binom{p+q}{p}|t_1|^2|t_2|^{2p+2}|r_1|^p|r_2|^q \tag{D.2}$$

is finite or infinite. Defining $x = |t_2|^2|r_1|$ and $y = |r_2|$, we may write Eq. (D.1) in the form

$$\rho' = |t_1|^2|t_2|^2\sum_{p=0}^{\infty}\sum_{q=0}^{\infty}\binom{p+q}{p}x^p y^q, \tag{D.3}$$

and since t_1 and t_2 are constants, it is sufficient to check the double sum

$$\rho'' = \sum_{p=0}^{\infty}\sum_{q=0}^{\infty}\binom{p+q}{p}x^p y^q > \sum_{p=0}^{\infty}\binom{2p}{p}(xy)^p > \sum_{p=1}^{\infty}\frac{(4xy)^p}{p}. \tag{D.4}$$

For the first inequality we used the fact that all terms in the sum are positive, and that, therefore, including only the diagonal terms in the sum provides a strict lower bound for the value of the sum, and for the second inequality we used the fact that $\binom{2p}{p} > 2^{2m}/m$, which is straightforward to show using the doubling formula for Euler's Γ function [71]. Analyzing the result in Eq. (D.4), we see that the sum over p converges for $xy < 1/4$. In this case, therefore, we cannot decide whether ρ'' is finite or infinite. For $xy = 1/4$, however, the last sum in Eq. (D.4) is the harmonic series, which diverges [71]. Therefore, for $xy = 1/4$, we definitely have $\rho'' = \infty$, which implies that in this case Eq. (5.1) is only conditionally convergent. Since for all $xy > 1/4$ the harmonic series provides a lower bound of the last sum in Eq. (D.4), we also have $\rho'' = \infty$ for all $xy > 1/4$. It follows that the ray sum in Eq. (5.1) is only conditionally convergent in all cases for which $z = |t_2|^2|r_1 r_2| \geq 1/4$. Finally, we have to answer the question whether $z \geq 1/4$ is possible at all. We note that $|r_1|$ may freely range between 0 and 1, while $|t_2|^2|r_2|$ can range only between 0 and $2/(3\sqrt{3})$, which is obtained by observing that $|t_2|^2 = 1 - |r_2|^2$ and subsequently determining the maximum of the function $w = (1 - |r_2|^2)|r_2|$. This implies that z may range between 0 and $2/(3\sqrt{3}) > 0.38$, which overlaps with $z > 1/4$. Thus, we have proved that an entire range of cases exists in which Eq. (5.1) is only conditionally convergent. In these cases of conditional convergence we are not allowed to sum rays in arbitrary order. As discussed in Sect. 5, in order to obtain correct results, we have to sum the rays in the order of increasing path length.

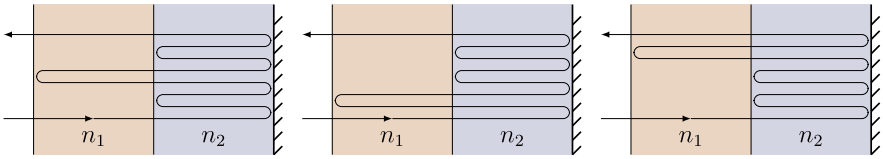

(a) $R_{1,2}$ (b) $R_{1,2}$ (c) $R_{1,2}$

Fig. D.1. Three ray trajectories that belong to the same class, $R_{1,2}$, and contribute with the same amplitude to the reflection amplitude of the film system. They differ only in the order of right-reflections on the vacuum/film and film/film interfaces. (a) The ray reflects inside the second film, then reflects inside the first film and reflects for the second time at the film/film interface and leaves the system. (b) The ray reflects once at the vacuum/film interface then enters the second film and reflects twice on the film/film interface. (c) The ray enters the second film, reflects twice on the film/film interface, enters the first film and reflects once on the vacuum/film interface.

References

[1] J. Krc, M. Zeman, S.L. Luxemburg, M. Topic, Modulated photonic-crystal structures as broadband back reflectors in thin-film solar cells, Appl. Phys. Lett. 94 (2009) 153501.

[2] P. Spinelli, A. Polman, Light trapping in thin crystalline si solar cells using surface mie scatterers, IEEE J. Photovolt. 4 (2) (2014) 554–559.

[3] Robin Vismara, Olindo Isabella, Miro Zeman, Back-contacted $BaSi_2$ solar cells: an optical study, Optic Express 25 (8) (2017) A402.

[4] Daniel Lockau, Tobias Sontheimer, Christiane Becker, Eveline Rudigier-Voigt, Frank Schmidt, Bernd Rech, Nanophotonic light trapping in 3-dimensional thin-film silicon architectures, Optic Express 21 (S1) (Jan 2013) A42–A52.

[5] Jonathan Grandidier, Dennis M. Callahan, Jeremy N. Munday, Harry A. Atwater, Light absorption enhancement in thin-film solar cells using whispering gallery modes in dielectric nanospheres, Adv. Mater. 23 (10) (2011) 1272–1276.

[6] M. Schmid, Review on light management by nanostructures in chalcopyrite solar cells, Semicond. Sci. Technol. 32 (4) (2017) 043003.

[7] C. Becker, P. Wyss, D. Eisenhauer, J. Probst, V. Preidel, M. Hammerschmidt, S. Burger, 5 by 5 cm^2 silicon photonic crystal slabs on glass and plastic foil exhibiting broadband absorption and high-intensity near-fields, Sci. Rep. 4 (2014) 5886.

[8] W.I. Nam, Y.J. Yoo, Y.M. Song, Geometrical shape design of nanophotonic surfaces for thin film solar cells, Optic Express 24 (14) (Jul 2016) A1033–A1044.

[9] Eli Yablonovitch, Statistical ray optics, J. Opt. Soc. Am. 72 (7) (1982) 899–907.

[10] Patrick Campbell, A. Martin, Green. Light trapping properties of pyramidally textured surfaces, J. Appl. Phys. 62 (1987) 243–249.

[11] T. Uematsu, M. Ida, K. Hane, Y. Hayashi, T. Saitoh, A new light trapping structure for very-thin, high-efficiency silicon solar cells, Photovoltaic Specialists Conference, 1988., Conference Record of the Twentieth IEEE, 1988, pp. 792–795.

[12] David Thorp, Stuart R. Wenham, Ray-tracing of arbitrary surface textures for light-trapping in thin silicon solar cells, Sol. Energy Mater. Sol. Cell. 48 (1997) 295–301.

[13] A.W. Smith, A. Rohatgi, S.C. Neel, Texture: a ray tracing program for the photovoltaic community, Photovoltaic Specialists Conference, 1990., Conference Record of the Twenty First IEEE, 1990, pp. 426–431.

[14] Rolf Brendel, Coupling of light into mechanically textured silicon solar cells: a ray tracing study, Prog. Photovoltaics Res. Appl. 3 (1995) 25–38.

[15] J.E. Cotter, Raysim 6.0 - a free geometrical ray tracing program for silicon solar cells, Photovoltaic Specialists Conference, 2005. Conference Record of the Thirty-first IEEE, 2005, pp. 1165–1168.

[16] Rudi Santbergen, Tomomi Meguro, Takashi Suezaki, Gensuke Koizumi, Kenji Yamamoto, Miro Zeman, Genpro4 optical model for solar cell simulation and its application to multijunction solar cells, IEEE J. Photovolt. 7 (2017) 919–926.

[17] Helmut Mäckel, Hendrik Holst, Mirko Löhmann, Eckard Wefringhaus, P. Pietro, Altermatt, Detailed analysis of random pyramidal surfaces with ray tracing and image processing, IEEE J. Photovolt. 6 (2016) 1456–1465.

[18] Hendrik Holst, Matthias Winter, Malte R. Vogt, Karsten Bothe, Marc Köntges, Rolf Brendel, P. Pietro, Altermatt, Applications of a new ray tracing framework to the analysis of extended regions in Si solar cell modules, Energy Procedia 28 (2013) 86–93.

[19] Keith R. McIntosh, Richard M. Swanson, Jeffrey E. Cotter, A simple ray tracer to compute the optical concentration of photovoltaic modules, Prog. Photovoltaics Res. Appl. 14 (2006) 167–177.

[20] Rolf Brendel, Simple prism pyramids: a new light trapping texture for silicon solar cells, Photovoltaic Specialists Conference, 1993., Conference Record of the Twenty Third IEEE, 1993, pp. 253–255.

[21] Garam Yun, Karlton Crabtree, Russell A. Chipman, Properties of the polarisation ray tracing matrix, Proc. SPIE 6682, Polarization Science and Remote Sensing III, 2007, p. 66820Z.

[22] Simeon C. Baker-Finch, Keith R. McIntosh, Reflection of normally incident light from silicon solar cells with pyramidal texture, Prog. Photovoltaics Res. Appl. 19 (2010) 406–416.

[23] Benjamin Lipovsek, Janez Krc, Marko Topic, Optical model for thin-film photovoltaic devices with large surface textures at the front side, Inf. MIDEM: J. Microelectron., Electron. Compon. Mater. 41 (4) (2011) 264–271.

[24] Janez Krc, Franc Smole, Marko Topic, Analysis of light scattering in amorphous si:h solar cells by a one-dimensional semi-coherent optical model, Prog. Photovoltaics Res. Appl. 11 (2003) 15–26.

[25] C. Zechner, P. Fath, G. Willeke, E. Bucher, Two- and three-dimensional optical Carrier generation determination in crystalline silicon solar cells, Sol. Energy Mater. Sol. Cell. 51 (1998) 255–267.

[26] Rolf Brendel, D. Scholten, Modeling light trapping and electronic transport of waffle-shaped crystalline thin-film si solar cells, Appl. Phys. A 69 (1999) 201–213.

[27] Simeon C. Baker-Finch, Keith R. McIntosh, One-dimensional photogeneration profiles in silicon solar cells with pyramidal texture, Prog. Photovoltaics Res. Appl. 20 (2012) 51–61.

[28] Keith R. McIntosh, Malcolm D. Abbotta, Ben A. Sudburya, Ray tracing isotextured solar cells, Energy Procedia 92 (2016) 122–129.

[29] M. Zworski, Semiclassical Analysis, Graduate Studies in Mathematics vol. 138, (2012).

[30] Reinhold Blümel, Advanced Quantum Mechanics: the Classical-quantum Connection, Jones & Bartlett Publishers, 2011.

[31] Janez Krc, Franc Smole, Marco Topic, One-dimensional semi-coherent optical model for thin film solar cells with rough interfaces, Inf. MIDEM: J. Microelectron., Electron. Compon. Mater. 32 (1) (2002) 6–13.

[32] Eugen Merzbacher, Quantum Mechanics, second ed. edition, Wiley, New York, 1970.

[33] L.D. Landau, Electrodynamics of Continuous Media, Volume 8 of Course of Theoretical Physics, second ed., Pergamon, Oxford, 1984 revised and enlarged by E.M. Lifshitz and L.P. Pitaevskii. edition.

[34] Jichi Ma, Jeff Chiles, Yagya D. Sharma, Sanjay Krishna, Sasan Fathpour, Two-photon photovoltaic effect in gallium arsenide, Optic Lett. 39 (18) (2014) 5297–5300.

[35] Sasan Fathpour, Kevin K. Tsia, Bahram Jalali, Two-photon photovoltaic effect in silicon, IEEE J. Quant. Electron. 43 (12) (2007) 1211–1217.

[36] V.E. Ferry, J.N. Munday, H.A. Atwater, Design considerations for plasmonic photovoltaics, Adv. Mater. 22 (43) (2010) 4794–4808.

[37] Richard Phillips Feynman, QED: the Strange Theory of Light and Matter, Princeton University Press, 2006.

[38] J.S. Townsend, Quantum Physics: a Fundamental Approach to Modern Physics, University Science Books, 2010.

[39] David J. Griffiths, Introduction to Electrodynamics, third ed. edition, Prentice Hall,

Upper Saddle River, N.J, 1999.
[40] R. Blümel, T.M. Antonsen, B. Georgeot, E. Ott, R.E. Prange, Ray splitting and quantum chaos, Phys. Rev. E 53 (Apr 1996) 3284–3302.
[41] A. Kohler, R. Blümel, Weyl formulas for quantum ray-splitting billiards, Ann. Phys. 267 (1998) 249–280.
[42] R. Blümel, P.M. Koch, L. Sirko, Ray-splitting billiards, Found. Phys. 31 (2001) 269–281.
[43] Martin C. Gutzwiller, Chaos in Classical and Quantum Mechanics, first ed. edition, Springer, 1990.
[44] L. Sirko, P.M. Koch, R. Blümel, Experimental identification of non-Newtonian orbits produced by ray splitting in a dielectric-loaded microwave cavity, Phys. Rev. Lett. 78 (Apr 1997) 2940–2943.
[45] Y. Hlushchuk, A. Kohler, Sz Bauch, L. Sirko, R. Blümel, M. Barth, H.-J. Stöckmann, Autocorrelation function of level velocities for ray-splitting billiards, Phys. Rev. E 61 (1) (2000) 366.
[46] N. Savytskyy, A. Kohler, Sz Bauch, R. Blümel, L. Sirko, Parametric correlations of the energy levels of ray-splitting billiards, Phys. Rev. E 64 (3) (2001) 036211.
[47] A. Kohler, R. Blümel, Annular ray-splitting billiard, Phys. Lett. A 238 (4–5) (1998) 271–277.
[48] A. Kohler, R. Blümel, Weyl formulas for quantum ray-splitting billiards, Ann. Phys. 267 (2) (1998) 249–280.
[49] A. Kohler, R. Blümel, Test of semiclassical amplitudes for quantum ray-splitting systems, Phys. Rev. E 59 (6) (1999) 7228.
[50] B. Riemann, Über die Darstellbarkeit einer Function durch eine trigonometrische Reihe, Dieterich, 1867.
[51] Stewart Galanor, Riemann's rearrangement Theorem, Math. Teach. 80 (8) (1987) 675–681.
[52] Seok-Joo Byun, Seok Yong Byun, Jangkyo Lee, Jae Wan Kim, Taek Sung Lee, Won Mok Kim, Young Kyu Park, Kyuman Cho, An optical simulation algorithm based on ray tracing technique for light absorption in thin film solar cells, Sol. Energy Mater. Sol. Cell. 95 (1) (2011) 408–411.
[53] H.S. Carslaw, A historical note on Gibbs' phenomenon in Fourier's series and integrals, Bull. Am. Math. Soc. 31 (8) (10 1925) 420–424.
[54] A. Nuttall, Some windows with very good sidelobe behavior, IEEE Trans. Acoust. Speech Signal Process. 29 (1) (Feb 1981) 84–91.
[55] Josefine K. Selj, David Young, Sachit Grover, Optimization of the antireflection coating of thin epitaxial crystalline silicon solar cells, Energy Procedia 77 (2015) 248–252 5th International Conference on Silicon Photovoltaics, SiliconPV 2015.
[56] A. Martin, Green. Self-consistent optical parameters of intrinsic silicon at 300K including temperature coefficients, Sol. Energy Mater. Sol. Cell. 92 (11) (2008) 1305–1310.
[57] D.T. Pierce, W.E. Spicer, Electronic structure of amorphous Si from photoemission and optical studies, Phys. Rev. B 5 (Apr 1972) 3017–3029.
[58] Tobias A.F. König, Petr A. Ledin, Justin Kerszulis, Mahmoud. A. Mahmoud, Mostafa A. El-Sayed, John R. Reynolds, Vladimir V. Tsukruk, Electrically tunable plasmonic behavior of nanocube–polymer nanomaterials induced by a redox-active electrochromic polymer, ACS Nano 8 (6) (2014) 6182–6192 PMID: 24870253.
[59] Reference solar spectral irradiance: Air mass 1.5. http://rredc.nrel.gov/solar/spectra/am1.5. (Accessed 19 April 2018).
[60] Max Born, E. Wolf, Principles of Optics: Electromagnetic Theory of Propagation, Interference and Diffraction of Light, fourth ed. edition, Pergamon Press, Oxford, 1970.
[61] John David Jackson, Classical Electrodynamics, second ed. edition, John Wiley & Sons, New York, 1970.
[62] Richard P. Feynman, Quantum Mechanics and Path Integrals, International Series in Pure and Applied Physics, McGraw-Hill, New York, 1965.
[63] R. Blümel, Yu. Dabaghian, R.V. Jensen, Explicitly solvable cases of one-dimensional quantum chaos, Phys. Rev. Lett. 88 (4) (January 2002).
[64] Yu. Dabaghian, R. Blümel, Explicit analytical solution for scaling quantum graphs, Phys. Rev. E 68 (Nov 2003) 055201.
[65] Yu. Dabaghian, R. Blümel, Explicit spectral formulas for scaling quantum graphs, Phys. Rev. E 70 (Oct 2004) 046206.
[66] Jiabao Zheng, Robert A. Barton, Dirk Englund, Broadband coherent absorption in chirped-planar-dielectric cavities for 2d-material-based photovoltaics and photodetectors, ACS Photonics 1 (9) (2014) 768–774.
[67] Jessica R. Piper, Shanhui Fan, Broadband absorption enhancement in solar cells with an atomically thin active layer, ACS Photonics 3 (4) (2016) 571–577.
[68] Yilei Li, Alexey Chernikov, Xian Zhang, Rigosi Albert, Heather M. Hill, Arend M. van der Zande, Daniel A. Chenet, En-Min Shih, James Hone, Tony F. Heinz, Measurement of the optical dielectric function of monolayer transition-metal dichalcogenides: Mos 2, mo s e 2, ws 2, and ws e 2, Phys. Rev. B 90 (20) (2014) 205422.
[69] Dario Cozza, Carmen M. Ruiz, David Duche, Sergio Giraldo, Edgardo Saucedo, Jean Jaques Simon, Ludovic Escoubas, Optical modeling and optimization of $Cu_2ZnSnSe_4$ solar cells using the modified transfer matrix method, Optic Express 24 (18) (2016) A1201–A1209.
[70] R. Blümel, Comment on 'quantum chaos in elementary quantum mechanics' by Yu. Dabaghian and R. Jensen, Eur. J. Phys. 27 (1) (2006) L1.
[71] I.S. Gradshteyn, I.M. Ryhzik, Table of Integrals, Series and Products, fifth ed., Academic Press, 1994.